SN Applied Sciences

Geometrically Nonlinear Deformation Reconstruction based on iQS4 Elements using a Linearized Iterative iFEM Algorithm

--Manuscript Draft--

Manuscript Number:	SNAS-D-22-01214
Full Title:	Geometrically Nonlinear Deformation Reconstruction based on iQS4 Elements using a Linearized Iterative iFEM Algorithm
Article Type:	Research Article
Abstract:	As an important research area of structural health monitoring, structural deformation monitoring can provide vital reference states for its system and ensure the safe operation of the structure in service. The inverse finite element method (iFEM) has been widely used as a practical method of structural deformation reconstruction thanks to its unique advantages. Current iFEM formulations have been applied to the small deformation of the structures based on the small-displacement assumption of the linear theory. However, this assumption may not be applicable to the structures with large displacements in practical engineering applications. Therefore, the geometric nonlinearity of structural deformation needs to be considered. In this study, to expand the practical utility of iFEM for large displacement monitoring, we propose a nonlinear iFEM algorithm based on the four-node inverse quadrilateral shell element, known as iQS4. Taking the advantage of an iterative iFEM algorithm, the nonlinear response is linearized to compute the geometrically nonlinear deformation reconstruction of the structure like the basic concept of nonlinear finite element analysis. Several examples are solved to verify the proposed approach. It is demonstrated that the large displacements can be accurately estimated even if the in-situ sensor data includes different levels of randomly generated noise. It is proven that the nonlinear iFEM algorithm provides more accurate displacement response as compared to the linear iFEM methodology for a complex structure undergoing large nonlinear deformations. Hence, the proposed approach can be utilized as a viable monitoring tool to effectively characterize geometrical nonlinear structural deformations of structures in real time.

Geometrically Nonlinear Deformation Reconstruction based on iQS4 Elements using a Linearized Iterative iFEM Algorithm

Mengying Li[1,*], Dawei Jia[1], He Huang[1,*] Ziyan Wu[1], Adnan Kefal[2,3,4]

[1]*School of Mechanics, Civil Engineering and Architecture, Northwestern Polytechnical University, Xi'an 710129, China*
[2]*Faculty of Engineering and Natural Sciences, Sabanci University, Tuzla, Istanbul 34956, Turkey*
[3]*Integrated Manufacturing Technologies Research and Application Center, Sabanci University, Tuzla, Istanbul 34956, Turkey*
[4]*Composite Technologies Center of Excellence, Istanbul Technology Development Zone, Sabanci University-Kordsa Global, Pendik, Istanbul 34906, Turkey*
**Corresponding author: hehuang0623@nwpu.edu.cn, myli1809@mail.nwpu.edu.cn*

Abstract: As an important research area of structural health monitoring, structural deformation monitoring can provide vital reference states for its system and ensure the safe operation of the structure in service. The inverse finite element method (iFEM) has been widely used as a practical method of structural deformation reconstruction thanks to its unique advantages. Current iFEM formulations have been applied to the small deformation of the structures based on the small-displacement assumption of the linear theory. However, this assumption may not be applicable to the structures with large displacements in practical engineering applications. Therefore, the geometric nonlinearity of structural deformation needs to be considered. In this study, to expand the practical utility of iFEM for large displacement monitoring, we propose a nonlinear iFEM algorithm based on the four-node inverse quadrilateral shell element, known as iQS4. Taking the advantage of an iterative iFEM algorithm, the nonlinear response is linearized to compute the geometrically nonlinear deformation reconstruction of the structure like the basic concept of nonlinear finite element analysis. Several examples are solved to verify the proposed approach. It is demonstrated that the large displacements can be accurately estimated even if the in-situ sensor data includes different levels of randomly generated noise. It is proven that the nonlinear iFEM algorithm provides more accurate displacement response as compared to the linear iFEM methodology for a complex structure undergoing large nonlinear deformations. Hence, the proposed approach can be utilized as a viable monitoring tool to effectively characterize geometrical nonlinear structural deformations of structures in real time.

Keywords: Deformation reconstruction; iQS4 element; iterative algorithm; nonlinear iFEM; structural health monitoring.

1. Introduction

Structural deformation monitoring is one of the key topics in the field of structural health monitoring. It can provide important reference information for structural health monitoring system, control system and fault diagnosis system to ensure the safe operation of the structure during service. ~~What's more,~~ it can realize a conditional maintenance and reduce maintenance cost. Therefore, there are several studies on shape sensing thus far. Among of them, three methods have been proved to be more effective and successful, including Ko's displacement theory, Modal Method, and inverse finite element method (iFEM). Compared with the other two methods, the iFEM has attracted extensive attention since it was proposed.

The iFEM was initially proposed by Tessler and Spangler [1] for plate and shell structures. A three-node triangular inverse-shell element iMIN3[2] was first~~ly~~ demonstrated by the minimization of a weighted-least-squares error functional between measured strain and theoretical strain. It is noteworthy that the method only makes use of limited strain data of measuring points and strain-displacement relations to reconstruct displacements. Most important of all, any materials properties or load information is unnecessary. At present, the iFEM has been widely used in deformation monitoring of many engineering structures. At the same time, in order to solve the inversion ~~algorithm~~ problem of different types of structures, a variety of inverse element models have been developed successively to further enrich the iFEM capability.

Cerracchio et al. [3] established a three-node triangular inverse finite element iRZT3 based on the ~~iFEM and the~~ improved zigzag theory for shape and stress monitoring of sandwich structures. Based on the iFEM, Gherlone et al. [4-7] put forward the shape sensing of some three-dimensional frame structures by a least square variational principle considering the section strain, involving tension, torsion, bending and transverse shear of Timoshenko theory. Kefal and Oterkus [8,9] proposed a quadrilateral inverse shell element iQS4 based on iFEM to expand the inverse shell element library and improve some deficiencies of iMIN3. It is applied to deformation monitoring of large ship hull and other marine structures [10,11] ~~so as~~ to obtain accurate

information about structural safety status in real time. Papa et al. [12] developed a triangular flat shell element iTRIA3 based on the iFEM for deformation reconstruction of three-dimensional shell and plate with the experimental verification on an equivalent plate model. Mooij [13] applied an inverse hexahedral solid element and a new standard set of benchmark problems of iFEM algorithm. Kefal [14] employed an efficient curved inverse-shell element iCS8 with a curved geometry to monitor displacement and stress of cylindrical offshore structures. To further compare the performance of different inverse elements, a detailed investigation was carried out on iFEM element iMIN3, iQS4 and iCS8 for structural shape and stress monitoring [15]. In addition, the iFEM was also used in other fields. For example, a two-dimensional deformation monitoring method was proposed by the iFEM of an iBeam3 element [16] for the pipeline in the process of soil freezing and thawing. Additionally, there are a few comparative studies involving common shape reconstruction methods. Esposito et al. [17,18] further discussed Modal Method, Ko's displacement theory and the iFEM simultaneously on shape sensing of a composite wing box, and the comparison was performed on the reconstruction deformation results in detail. Besides, to further develop the unique advantages of the iFEM, there are a few studies on structural damage identification recently. Some damage identification methods based on the iFEM were applied for damage localization [19-25] and damage quantification [26].

To summarize, the iFEM catches researchers' attention in recent years and has been proven to be successful for various fields in the existing literatures. It needs to point out that most of above review mainly study small-displacement assumption because the iFEM was originally based on linear theory. However, there are plenty of flexible structures such as solar arrays, tensional domes, suspension bridges and so on in practical engineering and ~~these~~ deformations of flexible structures generally have geometric nonlinear characteristics. Thus, it is inappropriate to still use the linear hypothesis to analyze, and the errors will far exceed the controllable range. ~~At this time~~, it should be discussed by the nonlinear theory. It seems that few applications of the iFEM to structural large-displacement problems were discussed in previous studies.

Tessler et al. [27] briefly introduced the range of applicability of the iFEM formulation. It is important to point out that nonlinear strain-displacement relations can replace the linear relations, or an incremental linear analysis method can be applied to simulate large displacement for geometrically nonlinear deformation problems. An inverse finite element strategy was implemented to recover large displacements of a cantilever beam, and it extended the linear iFEM formulation in some sense. However, this method only considered a two-dimensional plane model [28]. Tessler et al. [29] proposed an iFEM incremental algorithm for nonlinear deformations of a clamped square plate based on the iMIN3 element.

Aim of this work is to further study the shape reconstruction of large displacement problems based on the iFEM. This paper proposes a nonlinear iFEM strategy based on the basic principle of linearized iFEM theory and iterative algorithm. Iterative method is a classical algorithm to solve nonlinear problems. ~~That is,~~ the nonlinear responses are treated by linearization approximation. The paper is structured as follows. Section 1 briefly reviews the research results of the iFEM at present. In Section 2, the ~~investigated~~ formulations for element iQS4 of the nonlinear iFEM are described. In Section 3, two examples are employed with considering large-displacement problems to make the comparisons of the results. Finally, some concluding remarks and recommendations are stated for future research in Section 4.

2. Mathematical Background and Iterative iFEM Algorithm

As previously mentioned, the deformation analysis of some structures can be applied by small-displacement assumption~~, namely that it can be approximately linearized the calculation process.~~ Nevertheless, it is improper for some structures with strong nonlinear characteristics such as large displacement. Therefore, it should be discussed using geometric nonlinear theory. Herein, a brief description of the nonlinear iFEM is reported. The proposed method is presented based on the theoretical framework of linear iFEM in this work.

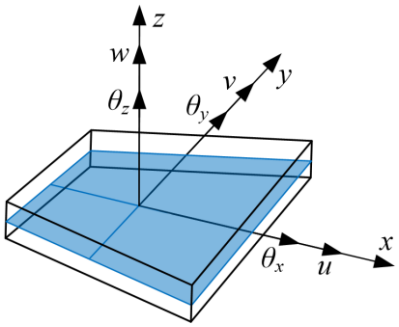

Fig.1 The 4-node quadrilateral inverse shell element, iQS4, with six degrees-of-freedom in global coordinates

~~As one of the most important methods to reconstruct structural deformation at present, some advantages of the iFEM are more favored.~~ There are different inverse elements based on the iFEM and the described iFEM approaches are valid for different types of structures. This paper focus on a four-node inverse quadrilateral shell element iQS4 as shown in Fig.1. The iQS4 was developed by Kefal et al. [9] and it has widely used to reconstruct deformation of various plate and shell structures. Because of the inclusion of drilling rotations θ_{zi}, it has less tendency toward shear locking. It is assumed that the iQS4 element has a thickness of $2h$ and that $z \in (-h, h)$ defines the thickness coordinate system. u_i and v_i are the positive x, y translations, respectively. θ_{xi}, θ_{yi} are positive clockwise rotations around the x, y-axes, respectively. Consequently, the elemental degrees-of-freedom vector $\mathbf{u}_i^e$ is formulated as follows:

$$\begin{aligned} \mathbf{u}_i^e &= \begin{bmatrix} u_i & v_i & w_i & \theta_{xi} & \theta_{yi} & \theta_{zi} \end{bmatrix}^T \left(i = 1,2,3,4\right) \\ \mathbf{u}^e &= \begin{bmatrix} \mathbf{u}_1^e & \mathbf{u}_2^e & \mathbf{u}_3^e & \mathbf{u}_4^e \end{bmatrix}^T \end{aligned} \tag{1}$$

The (x, y) coordinate in the reference plane of the iQS4 element is defined as a function of the bilinear shape function $N_i(s, t)$ with $(s, t) \in [-1, 1]$. The detailed expressions are summarized in [9]. The mapping functions are defined in Eq. (2). where, (x_i, y_i), $(i = 1, 2, 3, 4)$ is the element local nodal coordinates. (s, t) is the isoparametric dimensionless coordinate.

$$\begin{aligned} x\left(s,t\right) &\equiv x = \sum_{i=1}^{4} N_i x_i \\ y\left(s,t\right) &\equiv y = \sum_{i=1}^{4} N_i y_i \end{aligned} \tag{2}$$

The u and v membrane displacements are defined by

$$\begin{aligned} u(x,y) \equiv u &= \sum_{i=1}^{4} N_i u_i + \sum_{i=1}^{4} L_i \theta_{zi} \\ v(x,y) \equiv v &= \sum_{i=1}^{4} N_i v_i + \sum_{i=1}^{4} M_i \theta_{zi} \end{aligned} \tag{3}$$

where L_i, M_i are shape functions that define the relationship between drilling rotation and membrane displacement, respectively. The detailed forms are expressed in [9]. The transverse displacement w and the bending rotations θ_x, θ_y are defined by the positive z translation w_i and positive counterclockwise rotations θ_{xi}, θ_{yi}.

$$\begin{aligned} w(x,y) \equiv w &= \sum_{i=1}^{4} N_i w_i - \sum_{i=1}^{4} L_i \theta_{xi} - \sum_{i=1}^{4} M_i \theta_{yi} \\ \theta_x(x,y) \equiv \theta_x &= \sum_{i=1}^{4} L_i \theta_{xi} \\ \theta_y(x,y) \equiv \theta_y &= \sum_{i=1}^{4} L_i \theta_{yi} \end{aligned} \tag{4}$$

Based on the strain-displacement relations of linear elastic constitutive theory, the kinematic relations of iQS4 element are established based on the First order Shear Deformation Theory (FSDT). The strain components consist of membrane ~~section~~ strains, bending ~~section~~ strains and transverse-shear strains. These can be expressed in terms of the nodal degrees of freedom.

$$\begin{Bmatrix} \varepsilon_{xx} \\ \varepsilon_{yy} \\ \gamma_{xy} \end{Bmatrix} = \begin{Bmatrix} u_{,x} \\ v_{,x} \\ u_{,y} + v_{,x} \end{Bmatrix} + z \begin{Bmatrix} \theta_{y,x} \\ -\theta_{x,y} \\ \theta_{y,y} - \theta_{x,x} \end{Bmatrix} = \mathbf{e}\left(\mathbf{u}^e\right) + z\mathbf{k}\left(\mathbf{u}^e\right) = \mathbf{B}^m\mathbf{u}^e + z\mathbf{B}^k\mathbf{u}^e \tag{5}$$

$$\begin{Bmatrix} \gamma_{xz} \\ \gamma_{yz} \end{Bmatrix} = \begin{Bmatrix} w_{,x} + \theta_y \\ w_{,y} - \theta_x \end{Bmatrix} = \mathrm{g}(\mathrm{u}) = \mathrm{B}^g \mathrm{u} \tag{6}$$

where $\mathbf{u}^e$ is the nodal displacement vectors. The matrices of $\mathbf{B}^m$, $\mathbf{B}^k$, $\mathbf{B}^g$ consist of derivatives of shape functions concerning the membrane, bending and shear response, respectively.

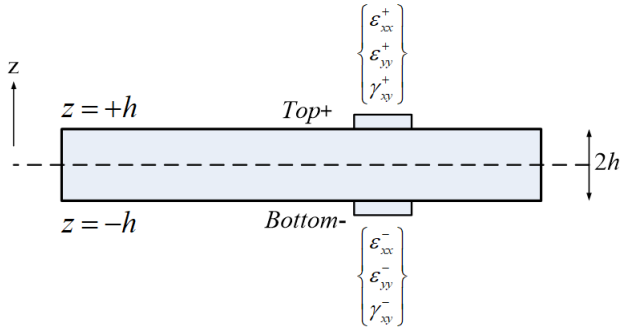

Fig. 2 Discrete surface strains measured at location $\boldsymbol{x}_i = (x, y)$

To further compute strain measurement relate to membrane and bending ~~section~~ strains, these can be evaluated from measured surface strains at n discrete locations. The stain sensors are placed on the top and bottom surfaces of the plate, as shown in Fig.2. Furthermore, the membrane and bending section strain at $\pm h$ from the middle of the element is shown in Eq. (7).

$$\mathbf{e}_i^{\varepsilon} = \frac{1}{2}\begin{Bmatrix} \varepsilon_{xx}^{+} + \varepsilon_{xx}^{-} \\ \varepsilon_{yy}^{+} + \varepsilon_{yy}^{-} \\ \gamma_{xy}^{+} + \gamma_{xy}^{-} \end{Bmatrix}_i \qquad \mathbf{k}_i^{\varepsilon} = \frac{1}{2h}\begin{Bmatrix} \varepsilon_{xx}^{+} - \varepsilon_{xx}^{-} \\ \varepsilon_{yy}^{+} - \varepsilon_{yy}^{-} \\ \gamma_{xy}^{+} - \gamma_{xy}^{-} \end{Bmatrix}_i \tag{7}$$

where the superscript '+'and '-' denote the strain measurements on the top and bottom surfaces, respectively. According to the deformation of thin shells, the $\mathbf{g}_i^{\varepsilon}$ can be neglected in the subsequent calculation due to much smaller contribution than $\mathbf{e}_i^{\varepsilon}$, $\mathbf{k}_i^{\varepsilon}$.

The core formulas of the iFEM are derived from the extreme value of the least-squares function between section strains and measured strains. It minimizes a weighted least-squares functional with respect to the unknown displacement degrees-of-freedom. Thus, the function for each element is expressed as follows

$$\Phi_e^{\lambda}\left(\mathbf{u}^e\right) = \omega_m \left\|\mathbf{e}(\mathbf{u}^e) - \mathbf{e}^{\varepsilon}\right\|^2 + \omega_k \left\|\mathbf{k}(\mathbf{u}^e) - \mathbf{k}^{\varepsilon}\right\|^2 + \omega_g \left\|\mathbf{g}(\mathbf{u}^e) - \mathbf{g}^{\varepsilon}\right\|^2 \tag{8}$$

$$\left\|\mathbf{e}(\mathbf{u}^e) - \mathbf{e}^{\varepsilon}\right\|^2 = \frac{1}{n}\iint_{A^e} \sum_{i=1}^{n} \left(\mathbf{e}(\mathbf{u}^e)_i - \mathbf{e}_i^{\varepsilon}\right)^2 dxdy \tag{9a}$$

$$\left\|\mathbf{k}(\mathbf{u}^e) - \mathbf{k}^{\varepsilon}\right\|^2 = \frac{(2h)^2}{n}\iint_{A^e} \sum_{i=1}^{n} \left(\mathbf{k}(\mathbf{u}^e)_i - \mathbf{k}_i^{\varepsilon}\right)^2 dxdy \tag{9b}$$

$$\left\|\mathbf{g}(\mathbf{u}^e) - \mathbf{g}^{\varepsilon}\right\|^2 = \frac{1}{n}\iint_{A^e} \sum_{i=1}^{n} \left(\mathbf{g}(\mathbf{u}^e)_i - \mathbf{g}_i^{\varepsilon}\right)^2 dxdy \tag{9c}$$

where ω_m, ω_k, ω_g are the positive weighting values associated with a given element. These weighting coefficients determine the extent to each theoretical strain components by constrained to measured values in the element. Moreover, these coefficients ensure stable performance even when strain values are not obtained from every finite element of the structure. Therefore, if every section strain element has a measured value, $\omega_m = \omega_k = \omega_g = 1$. Meanwhile, a value of 10^{-4} is given to each weighting coefficient when no strain values are taken for elements.

The unknown variable of the minimum error functional is the element node displacement in Eq. (8). According to the theory of variational principle, the condition for the minimum value of the functional is defined as

$$\frac{\partial \Phi_e^{\lambda}}{\partial \mathbf{u}^e} = \mathbf{k}^e \mathbf{u}^e - \mathbf{p}^e = 0 \tag{10}$$

$$\mathbf{k}^e = \iint_{A^e} \left(\omega_m (\mathbf{B}^m)^T \mathbf{B}^m + \omega_k (2h)^2 (\mathbf{B}^k)^T \mathbf{B}^k + \omega_g (\mathbf{B}^g)^T \mathbf{B}^g \right) dxdy \tag{11a}$$

$$\mathbf{p}^e = \frac{1}{n} \iint_{A^e} \sum_{i=1}^{n} \left(\omega_m (\mathbf{B}^m)^T \mathbf{e}_i^{\varepsilon} + \omega_k (2h)^2 (\mathbf{B}^k)^T \mathbf{k}_i^{\varepsilon} + \omega_g (\mathbf{B}^g)^T \mathbf{g}_i^{\varepsilon} \right) dxdy \tag{11b}$$

The Eqs. (11a-b) are the local iFEM matrix-vector equations, which can be assembled for the complete iFEM/iQS4 discretization like the classical finite-element assembly procedure. Then, the resultant global equation can be solved as

$$\mathbf{U}_i^e = \left(\mathbf{K}^e \right)^{-1} \mathbf{P}_i^e \tag{12}$$

where $\mathbf{U}_i^e$ is the displacement at *i* step within the total incremental step used in nonlinear shape-sensing calculation. $\mathbf{K}^e$ is a time-independent global pseudo stiffness matrix. It is only related to the shape function of the elements, which is different from the stiffness matrix in the finite element calculation. $\mathbf{P}_i^e$ is a function of measuring strain values, and it is updated in real time with iteration in the nonlinear iFEM program.

A schematic of the computing process of nonlinear iFEM is depicted in Fig.3(a) and the iterative process is observed in Fig.3(b). Considering the conversion of displacement-freedom from the local coordinate system to the global coordinate system, the standard FE integration operation is performed. The element matrix of a discrete structure is assembled into the linear equation system. Synthesizing the above formula leads to the structural global solution shown in Eq. (12).

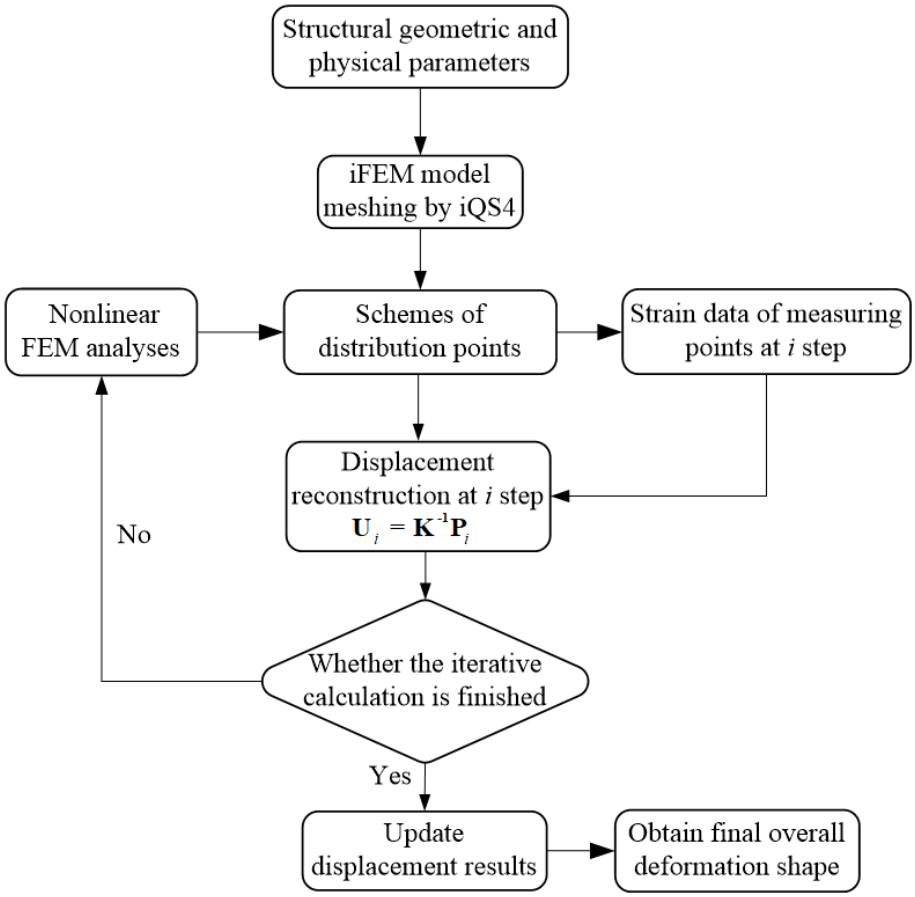

(a)

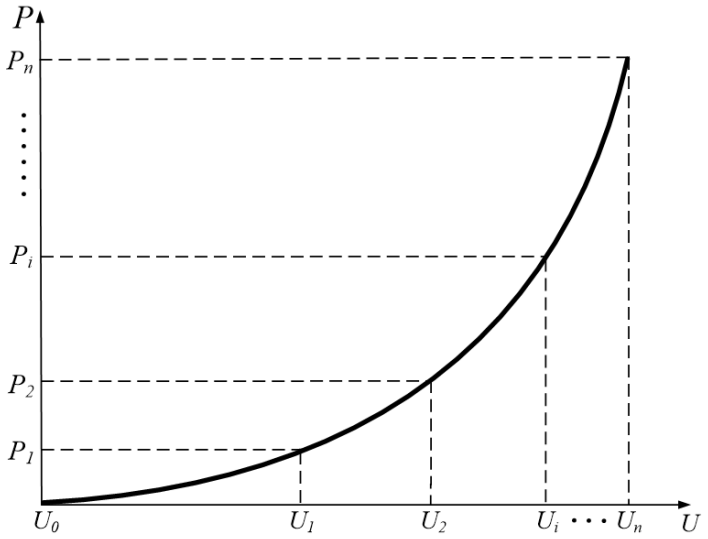

(b)

Fig. 3 The calculation process of large displacement reconstruction by the nonlinear iFEM. (a) a schematic of the computational process of nonlinear iFEM and (b) iterative calculation

The basic computing process of nonlinear iFEM method is illustrated as following,

(1) Firstly, the displacement components of inverse element iQS4 are formulated in Eqs. (3) and (4). The relevant matrices are formed ~~with~~ using Eqs. (5) and (6). The finite element model and inverse finite element model are established. Thus, the required parameters of the calculated structure are also determined. In this work, two models adopt the same mesh configuration.

(2) Secondly, a nonlinear FE calculation is carried out. The strains of measuring points are obtained as Eq. (7) under each incremental step in real time. It should be pointed that the strain is a total strain treating as the measured value in practical applications. In this work, the iFEM can still exert its merits although linear strain and nonlinear strain components are not separated in the case of large displacement analysis.

(3) Then, finite strain value from above Step (2) are taken as input data in Eq. 11(b) to execute the iFEM. As a result, the deformations $\mathbf{U}_i$ based on Eq. (12) at this time are reconstructed.

(4) Finally, Steps (2) and (3) are repeated until all iterative calculations are completed. The final overall deformation shape can be obtained from Fig.3(a).

In this paper, the linear iFEM theory is further modified. The algorithm model of the nonlinear iFEM is established by linearizing the nonlinear response analysis. For a nonlinear FE analysis, the load value P_i is determined when the iterative calculation of each incremental step is completed (in equilibrium convergence state). Concurrently, a set of corresponding strain data can be obtained. Then input the strain data from each step to execute the nonlinear iFEM program. Meanwhile, the deformation is reconstructed at each incremental step by Eq. (12). Until all iterative calculations are finished, all the shape information is finally summarized, and the real deflections of the structure are presented. Finally, the performance of above algorithm about linear iFEM and nonlinear iFEM can be evaluated by comparing the final deflection results.

3. Numerical examples

The effectiveness of the proposed method above is numerically demonstrated on a cantilever plate model and a stiffened plate. Herein, it needs to point out that the iFEM mesh adopts the same mesh configuration as the FE model mesh in the following.

3.1 A cantilever plate subjected to a uniformly distributed load

A cantilever plate is considered and the overall dimension is 0.7m×0.3m with a thickness of 12.5mm. The elastic modulus and Poisson's ratio of the plate are shown in Fig.4(a). The top surface of the cantilever plate is subjected to a uniformly distributed load (3MPa) and left edge is clamped. In this section, the required strain data of measuring points, selected as inputs to the nonlinear iFEM program, are all extracted from a nonlinear FE study. As a consequence, a high-fidelity FE model is established with 800 SR4 elements and 5166 DOFs shown in Fig.4(b).

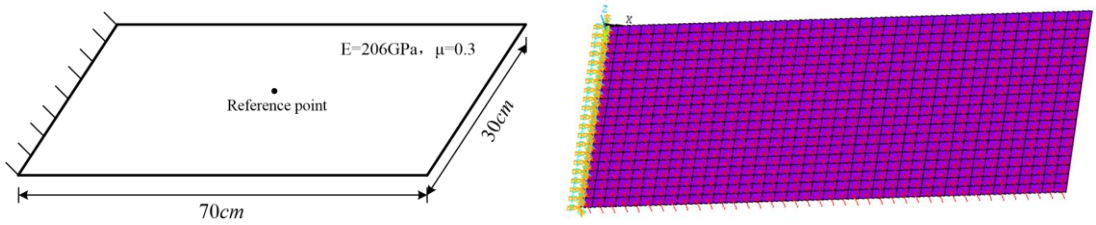

(a) (b)

Fig.4 A cantilever plate model. (a) geometrical dimensions and boundary conditions of a cantilever plate subjected to a uniformly distributed load and (b) a high-fidelity FE model as reference.

3.2 A stiffened plate (SP) subjected to a uniformly distributed load

Fig.5 shows a cantilever stiffened plate subjected to a uniformly distributed load (1MPa) which is clamped along the left edge. The geometric dimension of the stiffened plate with a thickness of 12.5mm is presented in the figure. The stiffened plate is composed of four ribs with a height of 0.03m and a thickness of 12.5mm. To further verify the effectiveness of the method, two different schemes of mesh are selected as the reference model for discussion, including a dense mesh and a coarse mesh. The

model in Fig.6(a) is named SP1152 which consists of 1152 SR4 elements and 7326 DOFs. Likewise, the model in Fig.6(b) is defined as SP126 which is composed of 126 SR4 elements and 900 DOFs.

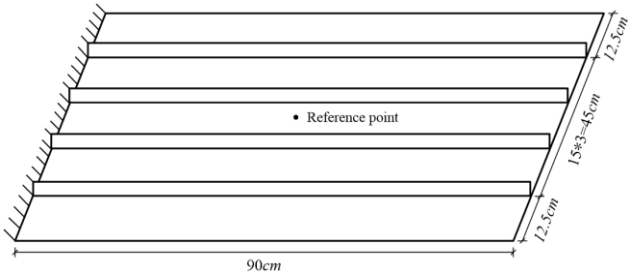

Fig.5 Cantilever stiffened plate subjected to a uniformly distributed load

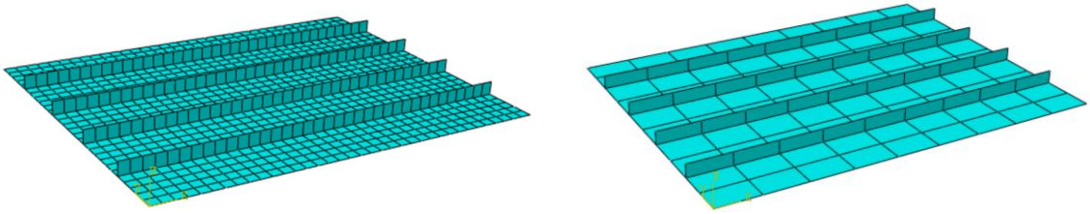

(a) (b)

Fig.6 Two mesh division schemes of stiffened plate model. (a) FE model with a dense mesh and (b) FE model with a coarse mesh.

4. Results

In this paper, the measured strains are both calculated from the centroid of each element of direct FE models. Meanwhile, there are several different configurations of measuring points to be calculated, including full distribution points and partial distribution points. Besides that, this work firstly discusses the influence of different levels of random noises on the reconstruction accuracy of large displacement problems. It simulates the inevitable errors effect in practical applications and the generality of this method is further discussed.

4.1 Discussion of the results for the cantilever plate

Fig. 8(a) shows the deformation reconstruction of ~~z displacement degree of freedom~~ *w*. It can be found that the large displacement can be effectively reconstructed

based on the nonlinear iFEM. What is discussed is the *z*-displacement of reference point marked in Fig.4(a) at the central position of the plate in this section. In Fig.8(b), a preliminary comparison produces the relative errors at zero between the reconstruction results with free noise and nonlinear FE results in previous steps and the maximum error is 4.7%. The change of curve is basically consistent. Contaminated by 3% random noise, the errors are below 0.5% and the maximum error is 4.8%. With the increase of noise level, the *z*-displacement curves are still in good agreement. Fig.8(b) shows that due to different noises pollution, the errors fluctuate around 1%.

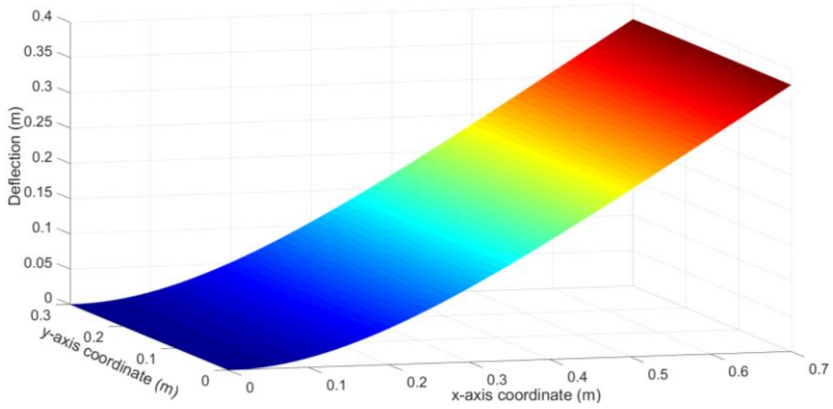

Fig.7 Displacement results of a cantilever plate FE model

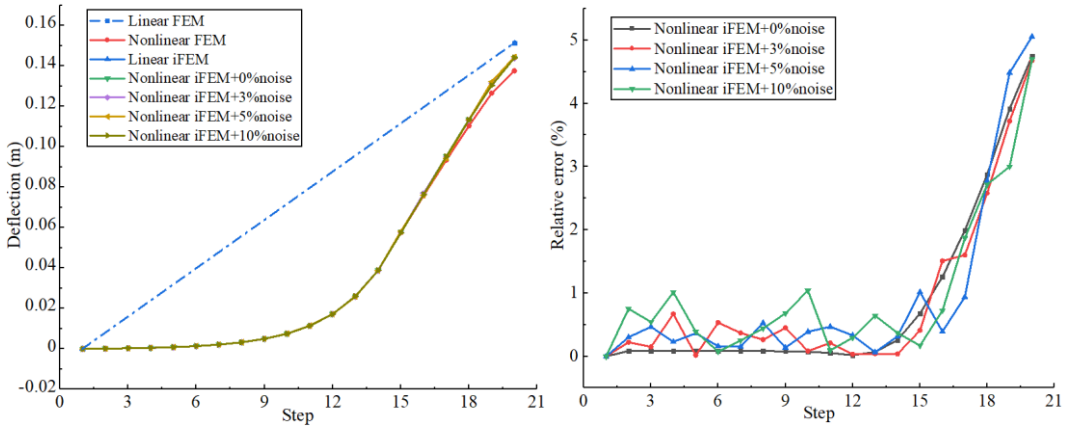

(a) (b)

Fig.8 The *z*-displacement reconstruction results at the center of cantilever plate under the nonlinear FEM, nonlinear iFEM with different random noises and linear iFEM analyses. (a) deflection results under different cases and (b) relative errors of Fig.8 (a)

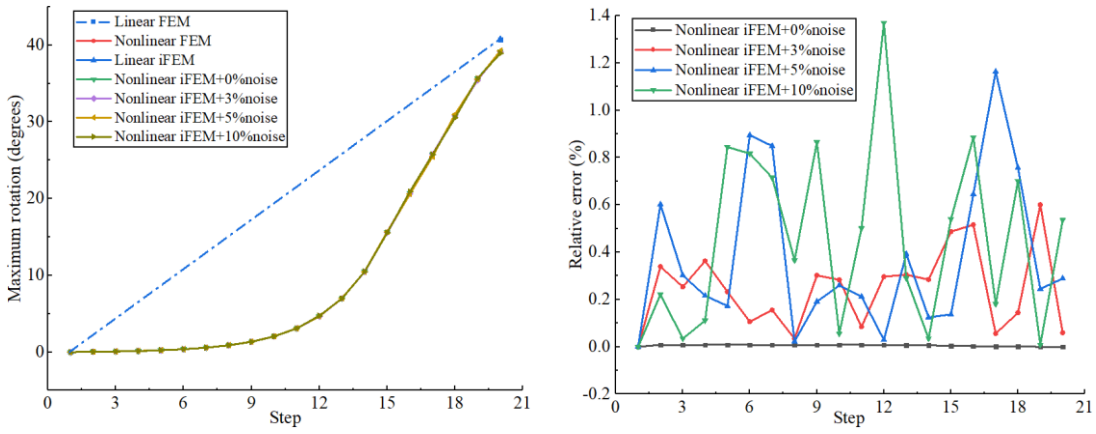

(a) (b)

Fig.9 Maximum *y*-axis rotation corresponding to the nonlinear FEM, nonlinear iFEM and linear iFEM. (a) maximum *y*-axis rotation and (b) relative errors of Fig.9(a)

In Fig.9(a), the reconstruction result of rotational degree of freedom θ_y is evaluated based on the nonlinear iFEM. As previously noted, the nonlinear iFEM can effectively reconstruct the rotation angle of the cantilever plate and update the angle value at each step. Furthermore, based on the curve of *y*-direction rotation angle, it can be judged that the cantilever plate model has undergone a large displacement and geometric nonlinearity is prominent. Compared with the reconstruction results of six degrees of freedom of all nodes, the change of rotational degree of freedom θ_y is the largest. Its reconstruction accuracy is higher than that of the displacement degrees of freedom. Similarly, after adding three different random noises of 3%, 5% and 10%, the reconstruction performance of the rotation degree of freedom θ_y are more ideal than that of the displacement degree of freedom *w*. Fig.9(b) plots that although polluted by different levels of random noise, overall reconstruction accuracy is high, that is, the relative errors are less than 1.4%. With the increase of the noise levels, the corresponding error curves appear a large fluctuation range.

4.2 Discussion of the results for the stiffened plate

Using the sensor placement models shown in Fig 10, the displacement of the reference point computed with nonlinear iFEM and linear iFEM at the center of the stiffened plate (marked in Fig.5) are compared in Figs. 11-12. Large displacement of the stiffened plate is effectively restructured based on the nonlinear iFEM and the results are basically consistent with the nonlinear FE analysis. The deformation shape reconstructed by the linear iFEM is a straight line from the initial point to the end point. There is a sharp contrast with the reconstruction results of nonlinear iFEM. On one hand, the results calculated by the linear iFEM differ greatly from the actual deformation, that is, the reconstruction error is large. On the other hand, the results based on the linear iFEM exhibit no nonlinear characteristics. To further estimate the generality of this method, strain data of measuring points are polluted by different random noises to simulate some inevitable errors in practical application. Herein, three different levels of noises 3%, 5% and 10% are mainly considered.

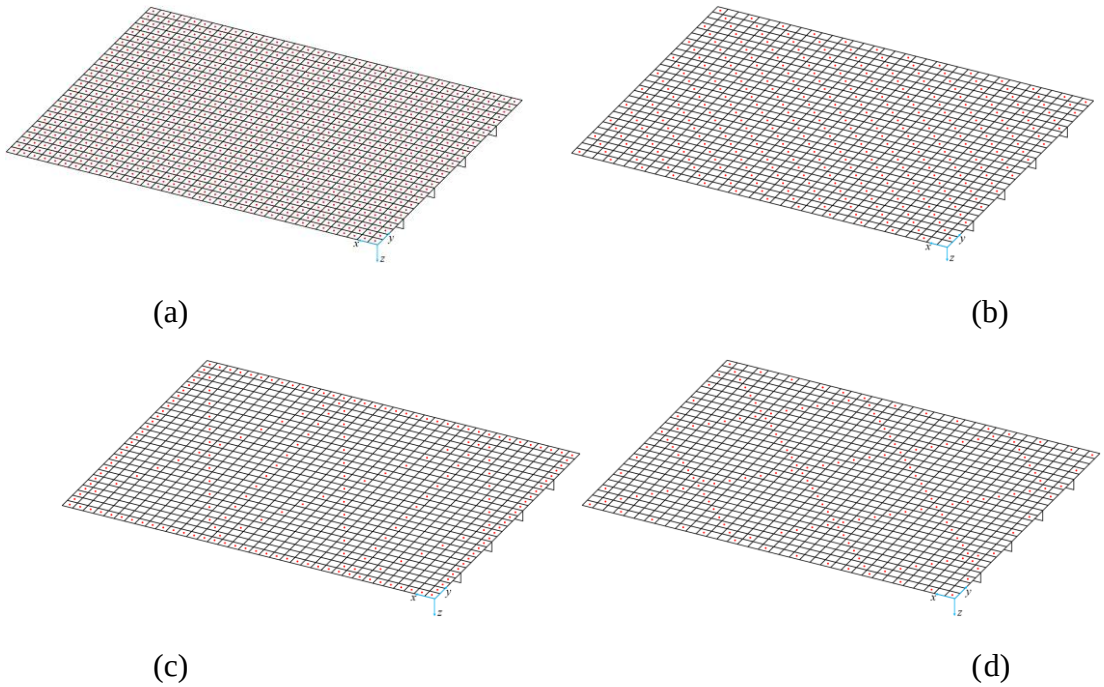

(a) (b)

(c) (d)

Fig.10 Different schemes of distribution points of iFEM model with a dense mesh. (a) an iFEM model named SP1152-1, (b) an iFEM model named SP1152-2, (c) an iFEM model named SP1152-3 and (d) an iFEM model named SP1152-4

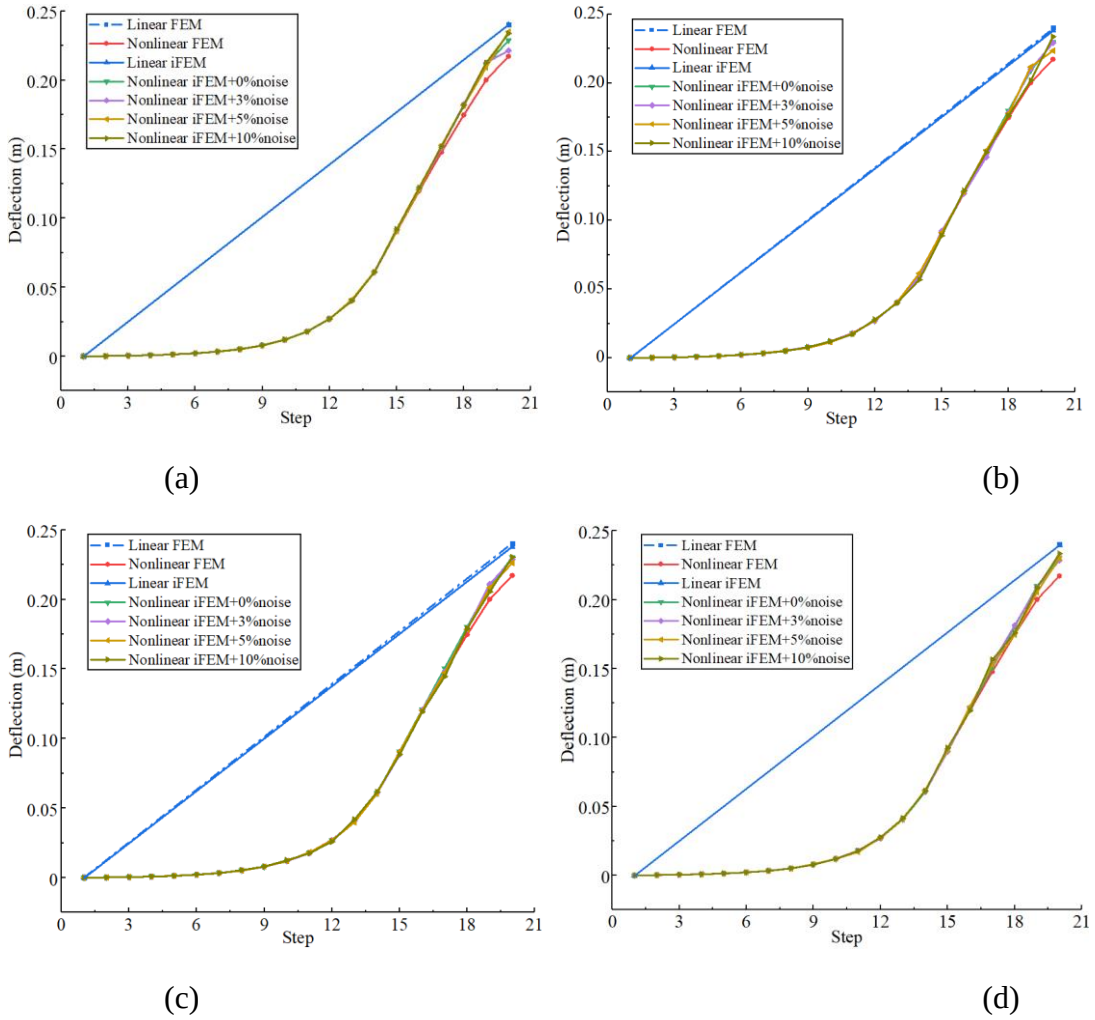

Fig.11 The results of *z*-displacement *w* at the center of stiffened plate by the nonlinear FEM and nonlinear iFEM with different random noises and linear iFEM analyses. (a) the deflections of SP11521-1, (a) the deflections of SP1152-2, (a) the deflections of SP1152-3 and (a) the deflections of SP1152-4

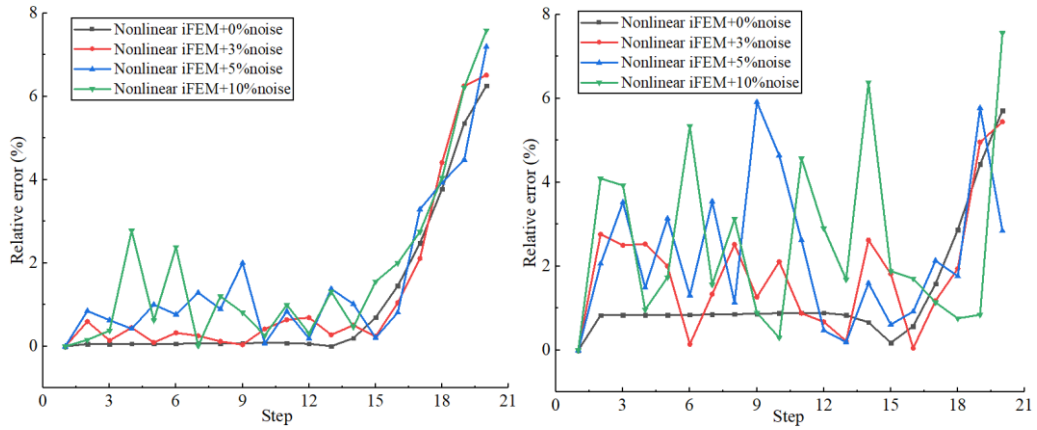

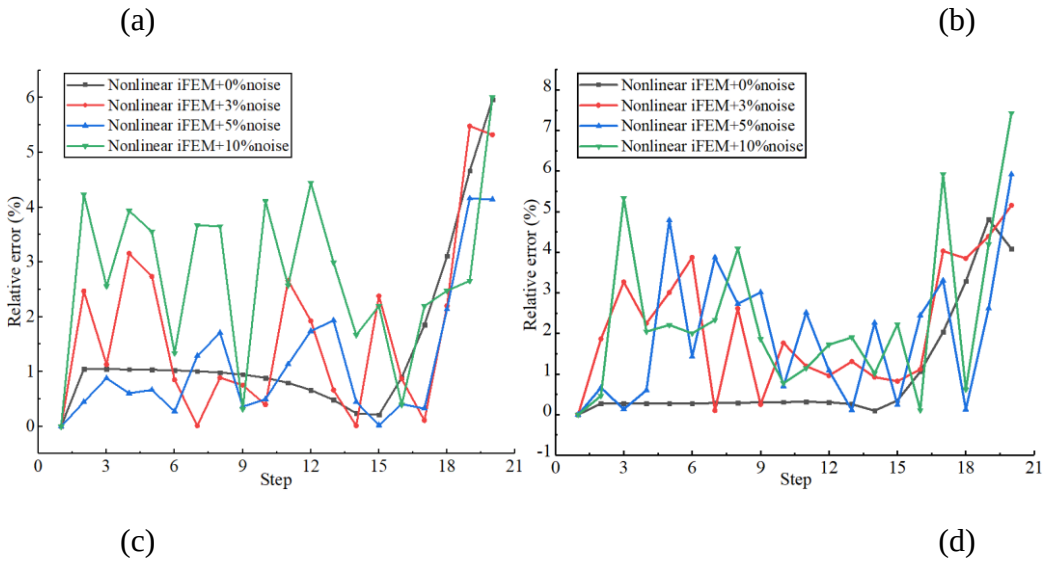

Fig.12 The errors comparison of different conditions between the nonlinear FEM and nonlinear iFEM with different random noises. (a) relative errors of SP1152-1, (b) relative errors of SP1152-2, (c) relative errors of SP1152-3 and (d) relative errors of SP1152-4

From the displacement results, it can be found that the results calculated by the nonlinear iFEM are consistent with nonlinear FE results in previous steps. It is demonstrated that even contaminated by different random noises the reconstruction accuracy still reaches an optimal level. Concurrently, Fig.12 report the relative errors of calculation results of the nonlinear iFEM in different cases. The best accuracy is obtained under free noise condition. With the progress of iterative calculation, the maximum error is 6.2%. Polluted by different random noises, the relative error curves of most of previous steps fluctuate obviously. Under the condition of 3% noise, the error curve fluctuates relatively small and is below 1%. The fluctuation range increases significantly with 5% and 10% noise, but both remain below 4%. It is the same as the case with no noise, the error reaches the maximum at the end of iteration. For example, the maximum reconstruction error is 7.8% when polluted by 10% random noise.

Given the previous considerations, four different schemes of distribution points of the coarse mesh configuration are taken into consideration to further verify the proposed method. In Fig.14, the reconstruction results of *z*-displacement are described under measuring points distribution of Fig.13. Compared with above dense mesh, the

reconstruction curves by the nonlinear iFEM and nonlinear FE results have the same behavior, although with a coarse mesh scheme. While accurately reconstructing deformation shape of the stiffened plate model, more importantly, it can effectively exhibit the geometric nonlinear characteristics. The linear iFEM presents a straight line between the initial point and the end point, and it seriously lacks the effective information of true deformation. What deserves attention is that the final reconstruction results are not affected by the roughness of mesh based on the nonlinear iFEM. Contaminated by different random noises, the reconstructed shape curves have a great fluctuation, but the geometric nonlinear information is still discovered from the displacement diagrams. Under polluted by 3% random noise, the reconstruction errors are < 3% and the maximum error is 5.1%. When the noise level is increased to 10%, the errors slightly below 5% are observed and maximum error reaches 5.4%. Above error results are within the controllable range. It is concluded that despite the pollution of noise, the nonlinear iFEM can still effectively restructure the deformation and geometric nonlinearity information.

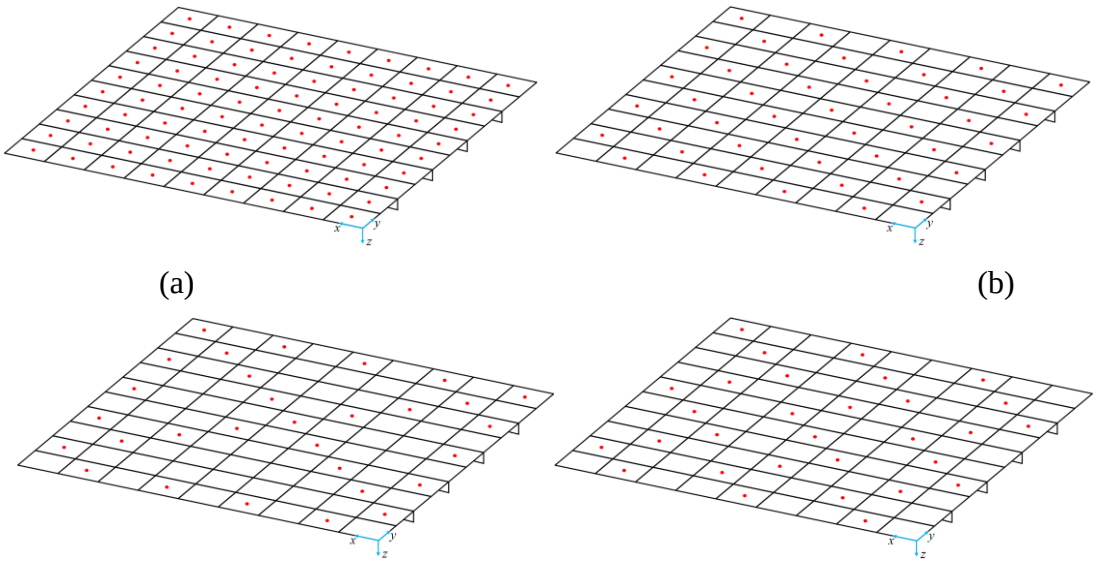

Fig.13 Different schemes of distribution points of iFEM model with a coarse mesh. (a) an iFEM model named SP126-1, (b) an iFEM model named SP126-2, (c) an iFEM model named SP126-3 and (d) an iFEM model named SP126-4

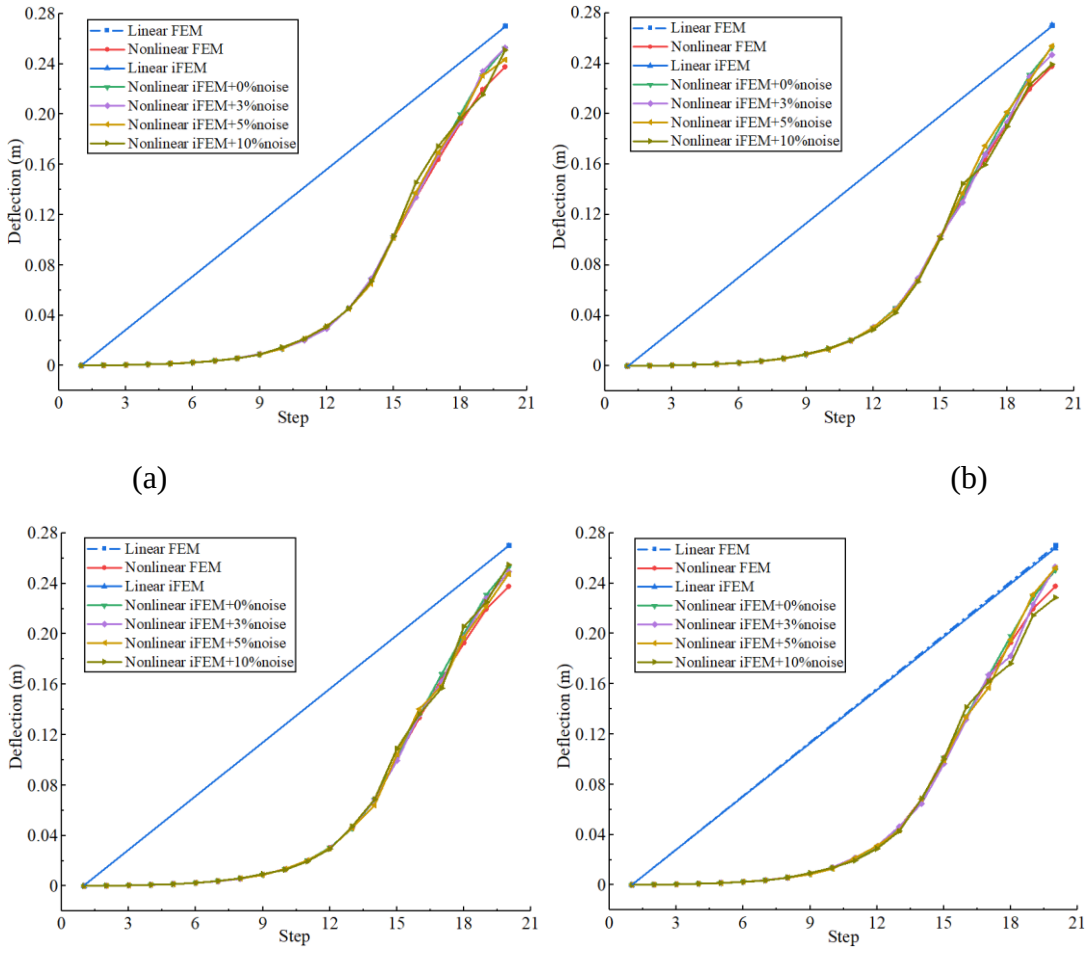

Fig.14 The results of *z*-displacement *w* at the center of stiffened plate by the nonlinear FEM and nonlinear iFEM with different random noises and linear iFEM analyses. (a) the deflections of SP126-1, (a) the deflections of SP126-2, (a) the deflections of SP126-3 and (a) the deflections of SP126-4

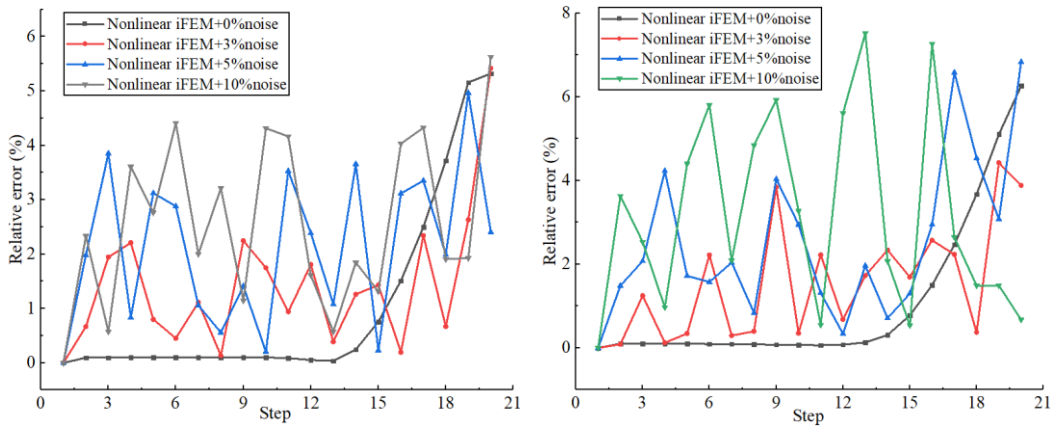

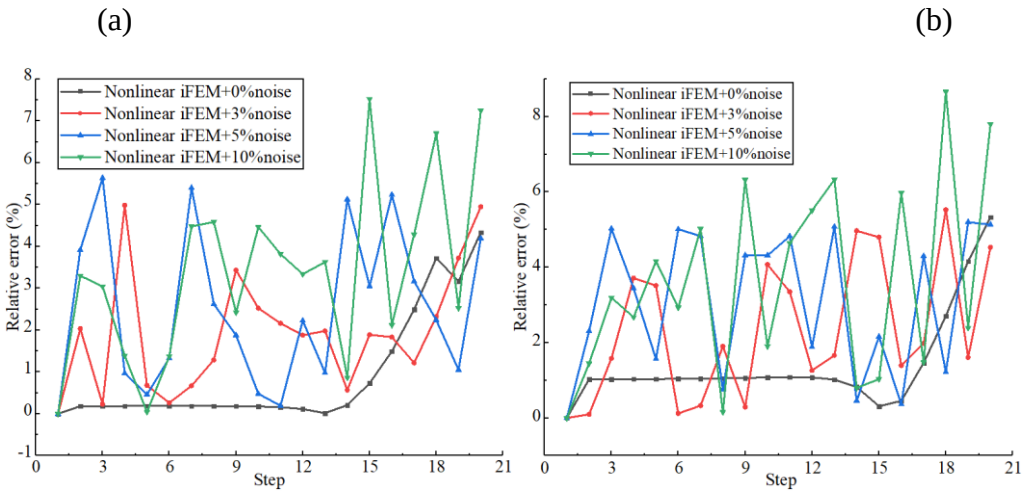

Fig.15 The errors comparison of different conditions between the nonlinear FEM and nonlinear iFEM with different random noises. (a) relative errors of SP126-1, (b) relative errors of SP126-2, (c) relative errors of SP126-3 and (d) relative errors of SP126-4

Secondly, the reconstruction results of measuring points distribution of two iFEM models SP126-3 and SP126-4 are depicted in Figs.14(c) and (d). The influence of noise pollution on its calculation results is considered at the same time. It is demonstrated that even with a few strain sensors the large displacements are reconstructed by nonlinear iFEM. Above figures depict that the deformation shape is effectively predicted by the nonlinear iFEM, and the geometric nonlinear characteristics are also displayed. Additionally, compared with a dense mesh of Fig.10(a) and a coarse mesh of Fig.13(a), the results are similar in the case of no noise, ~~that is, most errors are close~~. However, the deflection reconstruction curve of the coarse mesh scheme has a larger amplitude of fluctuation than that of dense mesh under the same noise level when affected by random noises. The calculation accuracy of the scheme of partial distribution points could not reach the level of the full distribution points, that is, the relative errors of the former are larger than the latter. From Fig.14, when relatively sparse measuring points are selected, the displacement reconstruction results can be effectively obtained by using the nonlinear iFEM. According to the analysis of above results, the distribution of measuring points at the boundary position has a great impact

on the reconstruction accuracy. It has the same performance in the reconstruction results of the model in Fig.10. In conclusion, large displacement can be effectively reconstructed by a few measured data, and the errors are basically below 10%.

Table 1 Comparison of final deformation between iFEM and FEM results

Model number	Accuracy estimation (%)	
	Nonlinear FEM vs. Linear iFEM	Nonlinear FEM vs. Nonlinear iFEM
SP1152-1	10.46	5.28
SP1152-2	9.60	5.71
SP1152-3	9.36	5.97
SP1152-4	10.23	6.09
SP126-1	13.61	6.32
SP126-2	13.84	6.26
SP126-3	13.51	6.30
SP126-4	12.55	5.33

Table 1 shows the accuracy estimation of the final deflection results of different stiffened plate model schemes. The effectiveness of the proposed method is further verified by comparing the results of linear iFEM, nonlinear iFEM and nonlinear FE calculation. It can be noticed that there is a large error between the calculation based on linear iFEM and nonlinear FE results. The differences produce an error $>10\%$. Nevertheless, the accuracy of displacement reconstruction is relatively high by using the nonlinear iFEM. An error of within 10% on above analysis is acceptable. From Table 1, SP1152 and SP126 can both achieve ideal accuracy based on the nonlinear iFEM. Even if a coarse meshing of the iFEM model is used, better reconstruction results can be estimated. Thus, it is concluded that large displacement reconstruction can be realized with less strain data. More than that, these results are closer to the real deformation of the model when geometric nonlinearity needs to be taken into consideration.

5. Conclusions

Based on the linear iFEM theory, a nonlinear inverse finite element method is proposed to realize the shape reconstruction of structures subjected to large displacement. Firstly, a few strain data at each incremental step is obtained by nonlinear FE calculation. They are used as the input to execute the iFEM program for further evaluating the displacement result at each iterative step until the end of all iterations. Then, the deformation information of all iterative steps is updated to describe the final shape. In this paper, a cantilever plate and a stiffened plate are considered for the analysis. There are two configurations of mesh generation of iFEM model, including a dense mesh and a coarse mesh, selected for discussion to further verify the effectiveness of this method.

This method makes full use of the unique advantages of the iFEM. On one hand, the change of structural shape can be restructured in real time with only a small amount of strain data obtained from measuring points. On the other hand, this method does not need to know the material properties and load parameters of the structure. Moreover, there is no need to distinguish between the linear elastic part of the strain and the part of geometric nonlinearity caused by large displacement, and the nonlinear iFEM still maintains the characteristics of iFEM program. Consequently, with the help of the basic concept of iterative method, this method not only reconstructs the displacement, but simultaneously presents the geometric nonlinear characteristics.

In this paper, to confirm the generality of this method, this work discusses the influence of different levels of random noises on the reconstruction results by the nonlinear iFEM for the first time. The results show that the large displacement problems can be effectively addressed. Compared with the previous studies, this method has been successfully applied to deformation reconstruction of three-dimensional plate structures by using the iQS4. Importantly, when dealing with nonlinear problems, the reconstruction accuracy of this method can be consistent with the actual situation. It can reach an acceptable accuracy of reconstruction although polluted by different levels of random noises.

Although the performance of the proposed method has been demonstrated, there are still some problems to be considered for a further analysis. For example, further works should point toward the accuracy comparison of different meshing schemes of iFEM model and different random noises on deflection. Furthermore, an exhaustive study on the influence of the configuration of sensors with respect to the capabilities of above algorithm should be assessed in future works.

Declaration of Competing Interest

The authors declare that they have no known competing financial interests or personal relationships that could have appeared to influence the work reported in this paper.

Acknowledgments

This research is supported by the National Natural Science Foundation of China (Grant No. 11902253) and the Fundamental Research Funds for the Central Universities of China. The authors are grateful for this support.

References

[1] A. Tessler, J.L. Spangler, A variational principal for reconstruction of elastic deformation of shear deformable plates and shells, NASA/TM-2003-212445, 2003.

[2] A. Tessler, J.L. Spangler, Inverse FEM for Full-Field Reconstruction of Elastic Deformations in Shear Deformable Plates and Shells, Proceedings of the 2nd European Workshop on Structural Health Monitoring, Munich, Germany, 7-9 July 2004.

[3] P. Cerracchio, M. Gherlone, Di Sciuva M, et al. A novel approach for displacement and stress monitoring of sandwich structures based on the inverse finite element method, Composite Structures, 127: 69-76, 2015.

[4] M. Gherlone, P. Cerracchio, et al. Dynamic shape reconstruction of three-dimensional frame structures using the inverse finite element method, Proceedings of 3rd ECCOMAS Thematic Conference on Computational Methods in Structural

Dynamics and Earthquake Engineering, Corfù, Greece, NASA/TP-2011-217315, 2011.

[5] M. Gherlone, P. Cerracchio, et al. Shape sensing of 3D frame structures using an inverse finite element method, International Journal of Solids and Structures, 49(22): 3100-3112, 2012.

[6] M. Gherlone, P. Cerracchio, et al. Beam shape sensing using inverse finite element method: theory and experimental validation, Proceeding of 8th International Workshop on Structural Health Monitoring, Stanford, CA, 2011.

[7] M. Gherlone, P. Cerracchio, M. Mattone, et al. An inverse finite element method for beam shape sensing: theoretical framework and experimental validation, Smart Materials and Structures, 23(4): 045027, 2014.

[8] A. Kefal, O. Hizir, E. Oterkus. A smart system to determine sensor locations for structural health monitoring of ship structures, Proceedings of the 9th International Workshop on Ship and Marine Hydrodynamics, Glasgow, UK. 2015: 26-28.

[9] A. Kefal, E. Oterkus, A. Tessler, et al. A quadrilateral inverse-shell element with drilling degrees of freedom for shape sensing and structural health monitoring, Engineering science and technology, an international journal, 19(3): 1299-1313, 2016.

[10] Li M Y, A. Kefal, B. Cerik, et al. Structural health monitoring of submarine pressure hull using inverse finite element method, Trends in the Analysis and Design of Marine Structures, 2019: 293-302.

[11] A. Kefal, E. Oterkus. Displacement and stress monitoring of a Panamax containership using inverse finite element method. Ocean Engineering, 2016, 119:16-29.

[12] U. Papa, S. Russo, A. Lamboglia, et al. Health structure monitoring for the design of an innovative UAS fixed wing through inverse finite element method (iFEM), Aerospace Science and Technology, 69: 439-448, 2017.

[13] De Mooij C, Martinez M, Benedictus R. iFEM benchmark problems for solid elements[J]. Smart Materials and Structures, 28(6): 065003, 2019.

[14] Kefal A. An efficient curved inverse-shell element for shape sensing and structural health monitoring of cylindrical marine structures, Ocean Engineering, 188: 106262, 2019

[15] Abdollahzadeh M A, Kefal A, Yildiz M. A comparative and review study on shape and stress sensing of flat/curved shell geometries using C^0-continuous family of iFEM elements, Sensors, 20(14): 3808, 2020.

[16] Wang J, Ren L, You R, et al. Experimental study of pipeline deformation monitoring using the inverse finite element method based on the iBeam3 element, Measurement, 2021, 184: 109881.

[17] M. Esposito, M. Gherlone. Composite wing box deformed-shape reconstruction based on measured strains: Optimization and comparison of existing approaches, Aerospace Science and Technology, 99: 105758, 2020.

[18] M. Gherlone, P. Cerracchio, M. Mattone. Shape sensing methods: Review and experimental comparison on a wing-shaped plate, Progress in Aerospace Sciences, 2018, 99: 14-26.

[19] C.C. Quach, S.L. Vazquez, et al. Structural Anomaly Detection Using Fiber Optic Sensors and Inverse Finite Element Method. AIAA Guidance, Navigation, and Control Conference and Exhibit15-18 August 2005, San Francisco, California, 2005.

[20] L. Colombo, C. Sbarufatti, M. Giglio, Anomaly identification in mechanical structures exploiting the inverse finite element method, Proceedings of the 6th European Conference on Computational Mechanics: Solids, Structures and Coupled Problems, ECCM 2018 and 7th European Conference on Computational Fluid Dynamics, ECFD 2018. 2020. 2234-2244.

[21] L. Colombo, C. Sbarufatti, M. Giglio, Definition of a load adaptive baseline by inverse finite element method for structural damage identification, Mechanical Systems and Signal Processing. 120 (2019) 584-607.

[22] L. Colombo, D. Oboe, C. Sbarufatti, et al, Shape sensing and damage identification with iFEM on a composite structure subjected to impact damage and non-trivial

boundary conditions, Mechanical Systems and Signal Processing, 148 (2021) 107163.

[23] M. Li, A. Kefal, B.C. Cerik, E. Oterkus, Dent damage identification in stiffened cylindrical structures using inverse Finite Element Method, Ocean Engineering, 198 (2020), 106944.

[24] H. Yang, Z. Wu, P. Sun, Strain Modal Method for Damage Detection Based on iFEM, Journal of Vibration, Measurement &Diagnosis. 37(1): 147-152, 205, 2017.

[25] M. Li, Z. Wu, H. Yang, H. Huang, Direct damage index based on inverse finite element method for structural damage identification, Ocean Engineering. 221 (14) 108545, 2021.

[26] M. Li, D. Jia, Z. Wu, et al. Structural damage identification using strain mode differences by the iFEM based on the convolutional neural network (CNN). Mechanical Systems and Signal Processing, 165, 108289, 2022.

[27] A. Tessler, J. L. Spangler. A least-squares variational method for full-field reconstruction of elastic deformations in shear-deformable plates and shells, Computer Methods in Applied Mechanics & Engineering, 194(2-5): 327-339, 2005.

[28] Krystian Paczkowski, H.R. Riggs. An Inverse Finite Element Strategy to Recover Full-Field, Large Displacements from Strain Measurements, ASME 2007 26th International Conference on Offshore Mechanics and Arctic Engineering. 2007.

[29] A. Tessler, Roy R, Esposito M, et al. Shape Sensing of Plate and Shell Structures Undergoing Large Displacements Using the Inverse Finite Element Method, Shock and Vibration, 2018, 2018:1-8.